Refinements to the Graves-Pitarka (GP) Kinematic Rupture Generator

Robert Graves *(USGS) and* ***Arben Pitarka*** *(LLNL)*

Poster: GM-218

Objectives

- The Graves-Pitarka (**GP**) kinematic rupture generator can quickly create realistic rupture descriptions for ground motion simulations and has long been a key component of **SCEC CyberShake** and **Broadband Platform** (**BBP**) projects.
- Recent refinements to the **GP** methodology are aimed at improving fidelity of simulated high-frequency (5-10 Hz) near-fault ground motions.
- Performance of the updated **GP** approach is examined by simulating near-fault ground motions (0 to 10 Hz) for a suite of M_w 7.0, 7.5, and 7.8 strike-slip events.

Refinements

- Incorporate depth-dependent slip-correlation lengths such that slip variation along the shallow portion of the rupture (upper 5 km) is considerably smoother than at depth.
- Scale local rise time directly with local slip and use average slip to determine average event rise time — prevents unrealistic dynamic stress drops.
- Develop down-sampling approach to reduce number of subfaults while preserving accurate representation of higher-frequency radiation — significant increase in computational efficiency for Green's function-based simulations.

Results

- Simulations show good agreement with spectral acceleration estimates from NGA-West2 ground motion models (GMMs) across period band of 0.1 to 10 s.
- Simulations also replicate observed frequency-dependent scaling of very near-fault (1-5 km) ground motions, including:
  - magnitude saturation of ground motions with increasing frequency
  - negative correlation of high-frequency ground motion level with increasing surface fault displacement (e.g., *Pinilla-Ramos and Abrahamson*, 2026).

Depth Dependent Slip Correlation Lengths

Models representing the magnitude (M_w) dependent along-strike (a_s) and down-dip (a_d) correlation lengths of shallow crustal earthquake slip distributions have been developed by *Somerville et al* (1999, **SEA99**), *Mai and Beroza* (2002, **MB02**) and *Suzuki et al* (2022, **SEA22**).

SEA99: $\log_{10} a_s = ½ M_w - 1.72$ $\log_{10} a_d = ½ M_w - 1.93$

MB02: $\log_{10} a_s = ½ M_w - 2.50$ $\log_{10} a_d = ⅓ M_w - 1.50$

SEA22: $\log_{10} a_s = ½ M_w - 1.67$ $\log_{10} a_d = ½ [\min(M_w, 6.3)] - 1.69$

While all studies used many of the same data, **MB02** exhibits significantly different scaling compared to **SEA99** and **SEA22**, which are nearly identical [**MB02** differs from others by a factor of $\log_{10}(2\pi)$]. **MB02** scaling worked well in previous ground motion studies (e.g., *Frankel*, 2009); however, it produces short length-scale slip variations inconsistent with observed surface fault offsets whereas **SEA99** and **SEA22** are generally consistent with observations.

To reconcile these differences, the updated **GP** utilizes a hybrid approach combining **SEA22** for depths shallower than 5 km and **MB02** for depths greater than 8 km, with linear interpolation from 5 to 8 km. This builds upon other depth-dependent features in the **GP** method that limit the strength of shallow high-frequency radiation, and also follows formulations where deeper, more compact asperity regions radiate the strongest motions (e.g., *Irikura and Miyake*, 2011; *Frankel*, 2017).

Panels at right show an M_w 7.0 example rupture with **MB02** scaling (top), **SEA22** scaling (middle), and hybrid/combined (bottom).

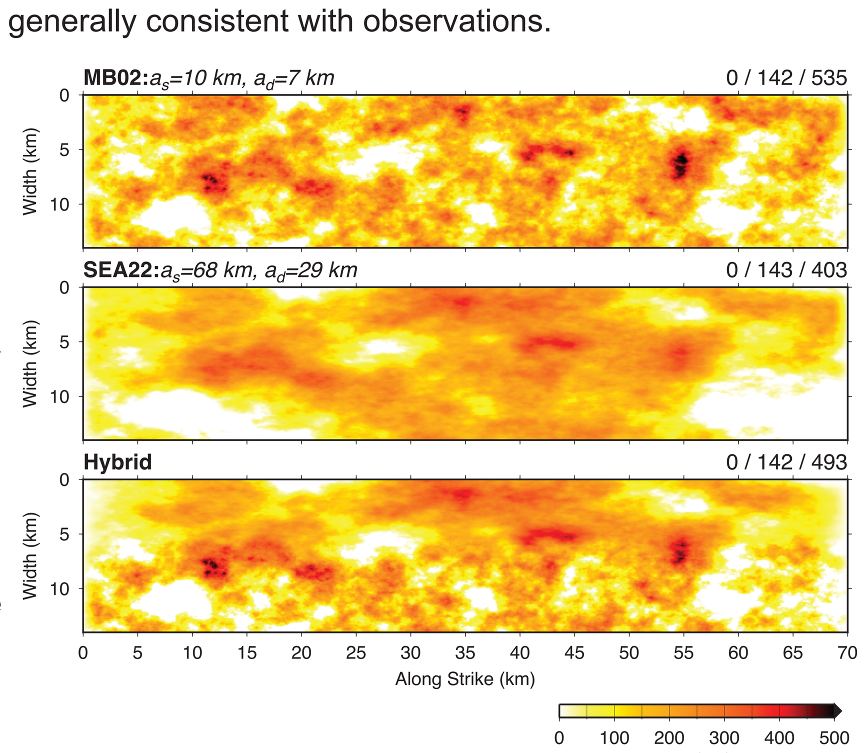

References

Aagaard, B., T. Brocher, D. Dolenc et al. (2008). Ground-Motion Modeling of the 1906 San Francisco Earthquake, Part I: Validation Using the 1989 Loma Prieta Earthquake, Bull. Seismol. Soc. Am. **98**, doi: 10.1785/0120060409.

Frankel A (2009) A constant stress-drop model for producing broadband synthetic seismograms: comparison with the next generation attenuation relations. Bull Seismol Soc Am **99**, 664–680. doi: 10.1785/01200 80079.

Frankel, A. (2017). Modeling strong-motion recordings of the 2010 Mw 8.8 Maule, Chile, earthquake with high stress-drop subevents and background slip, Bull. Seismol. Soc. Am. **107**, doi: 10.1785/0120160127.

Graves (2023). Characterization of Complex Kinematic Ruptures for Ground Motion Simulation, Abstract for SSA/SSJ Physics-Based Ground Motion Modeling Meeting, Vancounver, BC.

Graves R, and A. Pitarka (2016): Kinematic ground motion simulations on rough faults including effects of 3D Stochastic velocity perturbations, Bull. Seis. Soc. Am.,**106**, 2136–2153, doi:10.1785/0120160088.

Irikura, K. and H. Miyake (2011). Recipe for Predicting Strong Ground Motion from Crustal Earthquake Scenarios, Pure Appl. Geophys. **168**, doi: 10.1007/s00024-010-0150-9.

Ji, C., and R. J. Archuleta (2020). Two Empirical Double-Corner-Frequency Source Spectra and Their Physical Implications, Bull. Seismol. Soc. Am. **XX**,1–25, doi: 10.1785/0120200238.

Leonard, M. (2014). Self-Consistent Earthquake Fault-Scaling Relations: Update and Extension to Stable Continental Strike-Slip Faults, Bull. Seis. Soc. Am.,**104**, 2953–2965, doi: 10.1785/0120140087.

Mai, P. M., and G. C. Beroza (2002). A spatial random field model to characterize complexity in earthquake slip, J. Geophys. Res. **107**, no. B11, doi: 10.1029/2001JB000588.

Pinilla-Ramos, C. I., and N. A. Abrahamson (2026). Constraining Rupture-Generator Scaling Using Measured Surface Offsets, Near-Fault Ground Motions, and Rupture Dynamic Simulations, Bull. Seis. Soc. Am., **XX**,1–17, doi: 10.1785/0120250197.

Somerville, P. G., K. Irikura, R. Graves, S. Sawada, D. Wald, Y. Iwasaki, T. Kagawa, N. Smith, and A. Kowada (1999). Characterizing crustal earthquake slip models for the prediction of strong-ground motion, Seismol. Res. Lett. **70**, 59–80.

Suzuki, F., K. Kato, and T.Watanabe (2022). Spatial Complexity Characteristics of Fault Slip from Japanese Earthquakes Based on Self-Similar Models: Comparison with Worldwide Empirical Models, Bull. Seismol. Soc. Am. **112**, 1853–1870, doi: 10.1785/0120210273.

Average Risetime

Previous versions of **GP** determined average risetime (τ_a = risetime average across entire fault) using the cube root of seismic moment. This works well for median static stress drop ruptures, but produces very large ground motions for high static stress drop events.

Updated **GP** gets average risetime using fault-averaged slip (S_a), calibrated from *Leonard* (2014). This gives stronger scaling of risetime with static stress drop, producing roughly constant peak slip-rate.

Panels below show slip-rate functions and their spectra for M_w 7.5 and 7.7 ruptures. Both have the same rupture areas, so M_w 7.7 is high static stress drop event.

Cube-Root Moment Scaling

$$\tau_a = 2.3 \times 10^{-9} (M_o)^{1/3}$$

Average slip increases much faster than average risetime for high static stess drop events, resulting in large peak slip-rates (ground motions). Implies ever increasing dynamic stress drop, as well.

Average Slip Scaling

$$\tau_a = 1.1 \times 10^{-2} S_a$$

Average risetime increases directly with average slip independent of static stress drop. Increase in ground motion shifted to lower frequencies (implies constant dynamic stress drop).

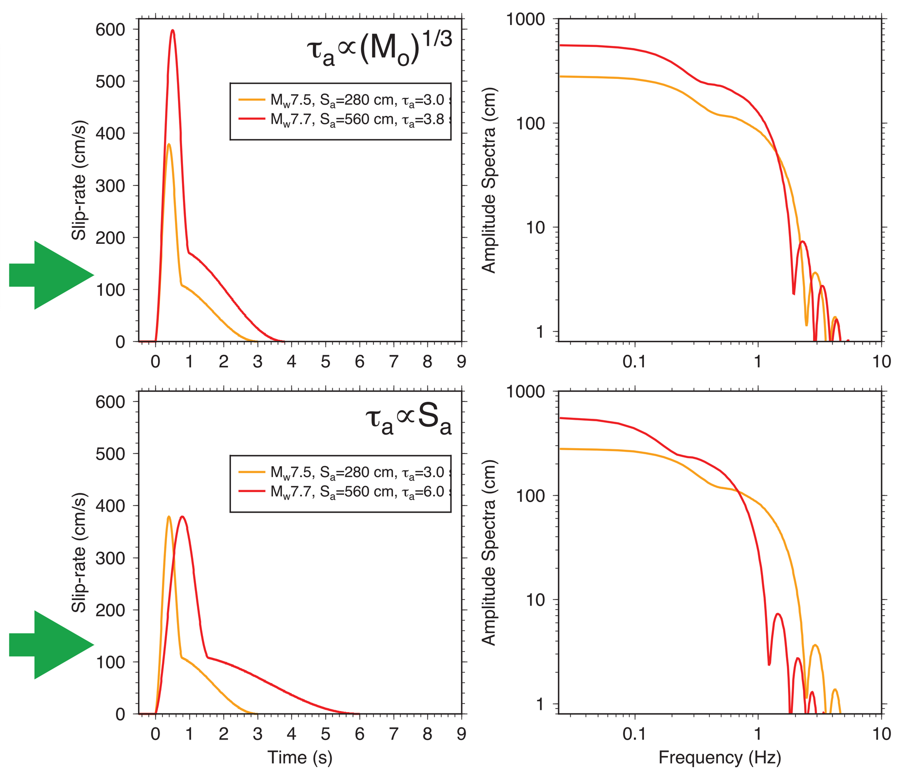

Local Risetime

Previous versions of **GP** scaled local risetime (τ_i = slip duration at subfault "i") with the square root of local slip (S_i = total slip at subfault "i"). While this formulation worked well in past applications (e.g., *Aagaard et al*, 2008), it has the undesireable feature of peak slip-rate increasing with increasing slip, which implies quite large dynamic stress drops for the largest slip values (e.g., *Tinti et al.*, 2005).

Updated **GP** adopts a formulation such that the local risetime scales directly with the local slip value (e.g., *Frankel*, 2009). This results in roughly constant peak slip-rate (implying roughly constant dynamic stress drop) across the entire rupture.

Below are slip-rate functions and spectra for a M_w 7.5 rupture. Average slip (S_a) is 280 cm, corresponding to the average risetime (τ_a) of 3.0 seconds and peak slip-rate of about 380 cm/sec.

Square-Root Slip Scaling

Regions of larger local slip experience increasingly larger peak slip-rates, thus implying ever increasing dynamic stress drop.

Direct Slip Scaling

All slip regions have roughly constant peak slip-rate (implying constant dynamic stress drop). Also, smaller slip values control higher frequency radiation, e.g., S_i=50 cm (gold curve).

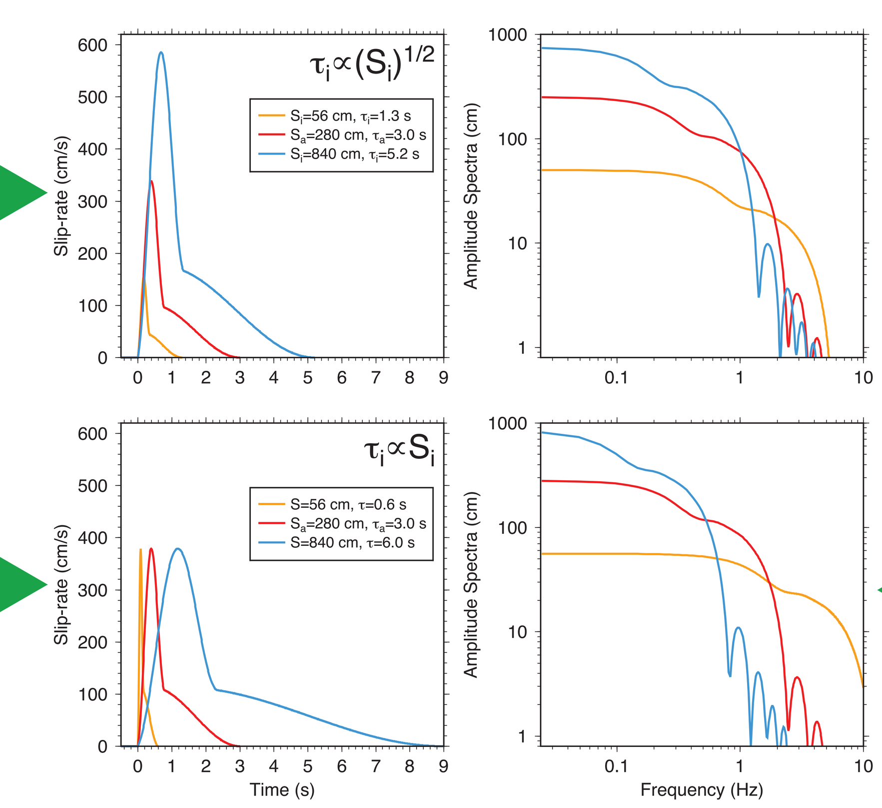

Examining Performance of Updated GP Method

The refined **GP** method was tested using deterministic broadband (0 – 10 Hz) simulations for surface-rupturing M_w 7.0, 7.5 and 7.8 strike-slip earthquakes (sampling multiple realizations with different slip distribution and rupture speed combinations). Green's functions (f_{NYQ} = 20 Hz) are for the **SCEC BBP** Loma Prieta region plane-layer (1D) velocity structure (V_{s30} = 500 m/s). In all realizations, three-component waveforms were simulated along profiles of stations located 1 km and 5 km from the surface expression of the fault.

Panels below compare RotD50 spectral acceleration simulated along the 5 km profile with estimates from four NGA-West2 ground motion models (GMMs). Median simulated value at each period is indicated by the blue square (error bars at +/-1 s.d.) and median values of the GMMs are shown in solid lines (dashed lines at +/-1 s.d.). Agreement between the simulations and GMMs is very good, with the exception of slightly lower simulated values at 0.3 to 0.5 sec, particularly for the larger magnitudes. This may result from ommission of 3D scattering effects in the simulations, which likely become more prevalent at large distance. Similar results are obtained for the 1 km profile.

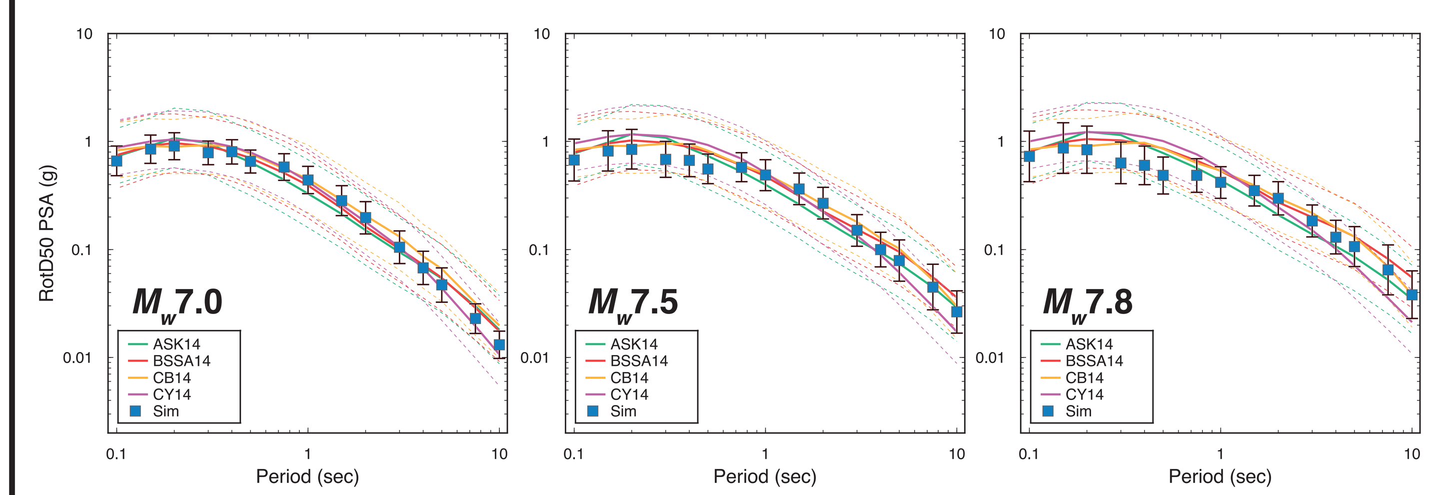

Frequency Dependent Ground Motion Scaling

For each realization, we determine normalized surface fault offset (surface slip divided by average fault slip) from the kinematic rupture at a location adjacent to each site. Peak intensity values at each site are then plotted as a function of normalized fault offset (panels below). Here, PGA, PGV, and PGD are proxies for high- (>3 Hz), mid- (0.3 - 3 Hz), and low- (<0.3 Hz) frequency bands.

The simulations exhibit an obvious frequency-dependent scaling of ground motion level as a function of surface fault offset. At low frequencies (PGD), ground motions show a strong positive correlation with fault offset and absolute ground motion levels show a clear magnitude dependence. At mid frequencies (PGV), the correlation is much weaker and the ground motion levels show a reduced dependence on magnitude. At high frequencies (PGA), the correlation between ground motion and fault offset is negative (consistent with observations of *Pinilla-Ramos and Abrahamson*, 2026), and there is little difference in absolute ground motion levels across magnitude ("magnitude saturation").

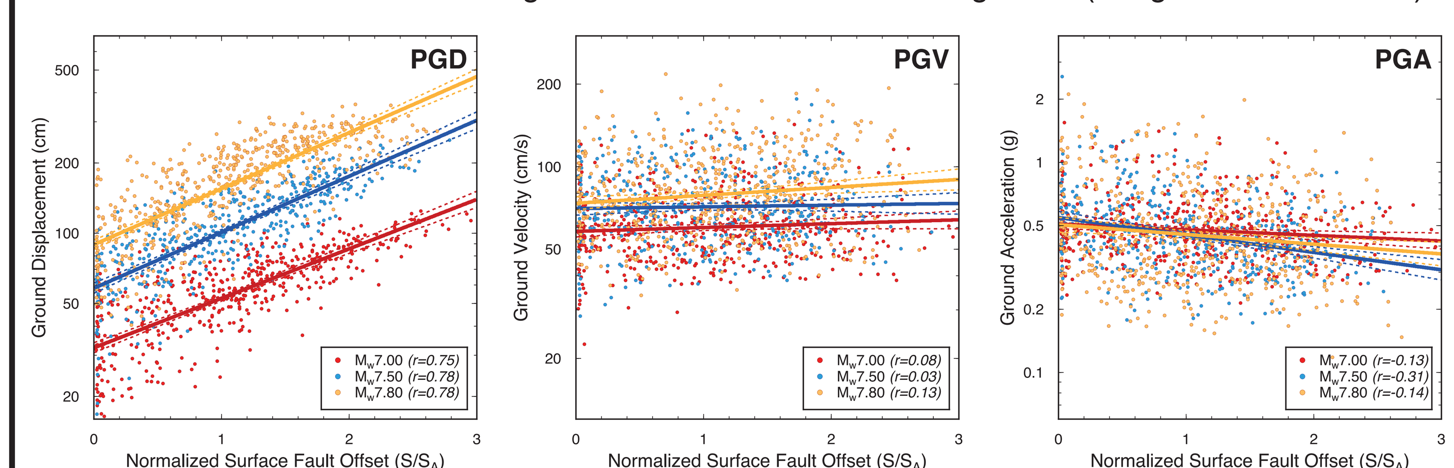

Why Should High Frequency Motions Negatively Correlate with Increasing Fault Offset?

The positive correlation of local slip with local risetime in the ***GP*** *method means higher frequency radiation (due to shorter risetime) will generally come from regions of smaller slip. While this won't necessarily be true in all earthquakes (especially buried ruptures) and can be influenced by other factors (e.g., scattering, attenuation, stochastic variations, etc.), it is not surprising that it occurs in the near-fault region of large magnitude surface rupturing events.*

Accurate Downsampling of Ruptures

Graves (2023) developed a relation between highest resolved frequency (f_{max}) and maximum useable subfault dimension (H_{max}) for the **GP** method: $H_{max} = 200 / f_{max}$, where H_{max} is in m. For f_{max} = 10 Hz, a subfault spacing of 20 m is required, which is computationally demanding, especially for Green's function based simulations. If larger subfaults are used, the higher frequencies are artifically boosted due to spatio-temporal aliasing where the starting and stopping of the rupture at each subfault appears discontinuous. Panels at the far right illustrate this using moment-rate functions of actual ruptures.

However, by accounting for the rupture time across the dense set of subfaults, the slip-rate functions can be downsampled to larger subfaults without significant loss of accuracy. This is illustrated at the lower left where a 5 x 5 grid of subfaults is downsampled to a single larger subfault. The slip-rate functions for the smaller subfaults are summed together in time producing a single slightly longer duration slip-rate function (lower right). The longer duration properly represents the rupture time across the subfault. The amplitude of the resulting slip-rate is scaled to produce the same seismic moment as the 5 x 5 grid, and the average strike, dip and rake are used for the larger subfault.

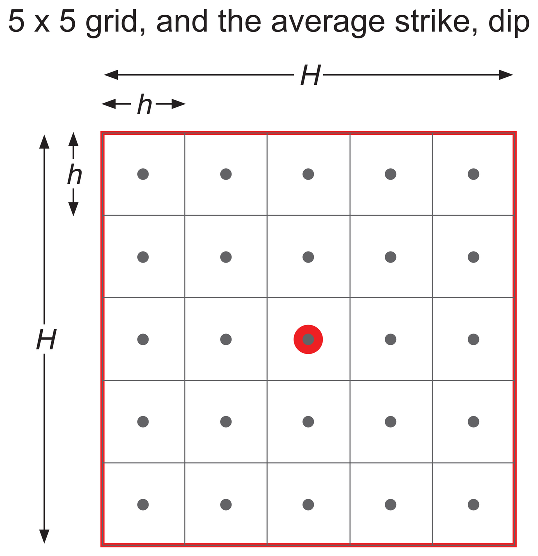

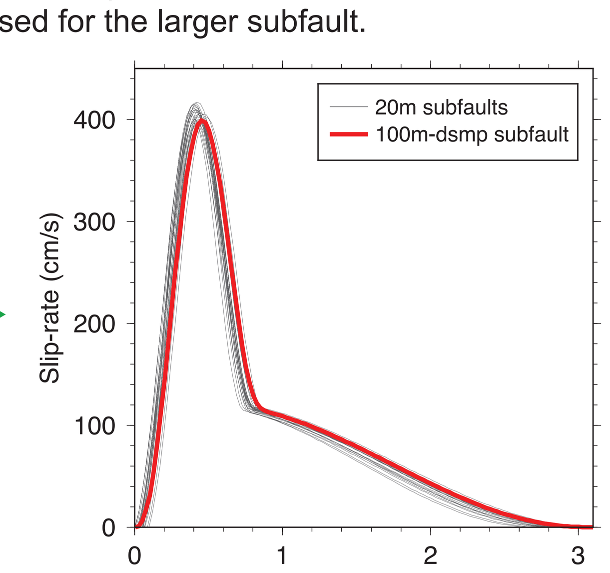

20 m Subfaults

M_w 7.0 moment-rate spectra exhibit expected f^{-2} falloff out to 10 Hz and beyond, consistent with theoretical model of Ji and Archuleta (2020).

100 m Subfaults

Creating identical ruptures as above but sampled at 100 m subfaults shows significant elevation of radiated energy beyond about 2 Hz due to aliasing effects.

Downsampling 20 m to 100 m Subfaults

Downsampling approach properly represents higher frequency radiation resulting in nearly identical spectra to the 20 m case.